Statistical and Dimension Reduction Methodology for Detecting and Parametrizing Core-Collapse Supernovae

Samuel Gailliot, B.S. The Ohio State University

A Master's Thesis submitted to the faculty of the Graduate School in partial fulfillment of the requirements for the degree of Master of Science in Applied Statistics

April 2020
Marquette University
Milwaukee, WI

Abstract

This paper explores statistical and dimension reduction methodology in the context of detecting and parametrizing gravitational wave signal from core collapse supernovae. Gravitational wave interferometer signals are simulated using a noise model which seeks to match the true detector noise. Using template matching, these noisy signals are tested to see if the underlying waveform can be detected. Then, using PCR the locations of interest within the signals are reconstructed and hypothesis tests for significance of coefficients are performed. While parameter estimation by way of hypothesis tests on significance of constituent waveforms shows limited usefulness, template matching is shown to be a useful and efficient method even within this context.

Contents

1 Introduction

Recently in physics, Einstein's general theory of relativity has been experimentally verified via the detection of gravity waves traveling through the fabric of the universe by the Laser Interferometer Gravitational Wave Observatory (LIGO). Creation and implementation of statistical methodology for the purposes of detecting gravitational waves has long been a focus of the LIGO scientific collaborative. While inspiral signals, those created by the mergers of compact binaries such as black holes and neutron stars have been detected, burst signals from core collapse supernova have yet to be discovered. I will summarize the problem and review methods that have been useful in detecting signature gravity waveforms. Subsequently, I will generate noisy simulated core collapse supernovae data streams with embedded signature waveforms. Template matching will be used to detect candidate locations of interest in noisy data streams. Once candidate locations of interest are identified, principal component regression (PCR) will be used to test the likelihood that these locations are signal from specific core collapse supernovae subtypes. Once PCR has been performed, the underlying signals can be reconstructed. Then, these reconstructions will be tested for similarity with understood simulations.

2 Background

2.1 Gravitational Wave Astronomy

2.1.1 Gravitational Waves

In 1916 Albert Einstein published his general theory of relativity, a geometrical theory of gravity.[Einstein, 1916] This theory posits that gravity arises from a curvature in a four dimensional manifold called space-time and conversely that space-time is curved in the presence of mass, energy, pressure and angular momentum. Like a bowling ball on a rubber sheet, a massive object like the sun deforms space-time. A smaller object, like the Earth, will move in orbit around the massive object in a geodesic along curved space-time, following the shortest path. In the words of physicist John Wheeler, mass tells space-time how to curve, and space-time tells mass how to move.[Misner et al., 1973]

Gravitational waves arise as a consequence of Einstein's theory. Gravitational waves are ripples in space time caused by the acceleration of massive objects which propagate through the universe at the speed of light. They stretch and compress space-time orthogonal to the direction of propagation. Their units are called strain, which is a dimensionless combination of two polarizations: a plus (+)-polarization and a cross (×)-polarization. Gravitational waves are also very weakly interacting. This is beneficial because they travel through the universe unobscured by intervening matter and remain a pure source of astrophysical information. By the time they reach the Earth, they have very small strain on space and only signals from hugely massive events are large enough for detection. Sources are expected to produce a strain of order h$\approx 10^{-21}$ which corresponds a displacement of approximately 10^{-18}, much smaller than the width of a proton, in the ground-based laser interferometers. This distance, relative to the length of the interferometers, is akin to the width of a human hair placed between the Earth and the moon. It is an amazing feat of engineering that the detectors are sensitive enough to directly detect gravitational waves from even the most massive events, inspiral events from coalescing black holes and neutron stars. GW150914, the first direct observation of gravitational waves, was an event of this type, but inspiral events are not the only source of gravitational waves.[Abbott et al., 2016b]

Gravitational waves are classified into four groups: inspiral, continuous, burst, and stochastic. Inspiral signals occur when two massive objects, black holes or neutron stars, fall into orbit. As the two massive objects orbit each other, they emit gravitational waves and lose energy. As they lose energy their orbital distance decreases which increases or-

bital and gravitational wave frequency as well as gravitational wave amplitude. This type of signal is the best understood and most well-modeled source of gravitational waves. Continuous gravitational waves are generated by single massive objects like pulsars (slightly aspherical, rapidly rotating neutron stars). These signals will generally be relatively weak, long-duration, and with near constant amplitude and frequency. Burst gravitational waves are high amplitude, short-duration events. Burst signals are expected to come from many sources, including: core collapse supernovae, cosmic string cusps, pulsar glitches, starquakes from magnetar flares, as well as yet unknown sources.[Edwards, 2017] Finally, Stochastic gravitational waves are the sum of small unresolved gravitational wave signals. Like the microwave background, the stochastic gravitational wave background could be left over from the Big Bang.[Romano and Cornish, 2017] Direct measurement of the stochastic gravitational wave background will allow researchers to see back to seconds after the Big Bang which will help constrain cosmological models of the early universe. Unfortunately, the stochastic gravitational wave background has the smallest strain and will be very difficult to detect.

Detection of inspiral signals is now, for the most part, a solved problem. Optimal parameter estimation in a Bayesian framework and template matching based search methods are well-defined for compact binary coalescence (CBC) signals.[Abbott et al., 2016a] On the other hand, it is most likely infeasible to detect continuous and stochastic gravitational wave signal using ground based detectors due to high levels of terrestrial noise. This leaves only the possibility of detecting burst signals. The most promising source of burst gravitational wave signals are core collapse supenovae. This would be scientifically interesting because, unlike electromagnetic observations which can only directly probe the envelope of a star, gravitational waves are emitted deep in the core of a collapsing star and travel unobscured across the Universe. Observation and measurement of gravitational waves from stellar core collapse will allow for insights about the core collapse dynamics and supernova mechanisms which could lead to theoretical developments.

2.1.2 Core Collapse Supernovae

Main Sequence stars, such as our Sun, convert hydrogen to helium through nuclear fusion in the core and release energy. When a star is much more massive than our Sun gravity causes the core to heat up enough to fuse heavier elements in the order: carbon, oxygen, neon, magnesium and finally iron. As elements fuse and release energy there is an outward

thermal pressure that balances the inward pull of gravity, like the air in a balloon. This outward push and inward pull in all directions is why stars have a spherical shape.

The lives of stars larger than eight solar masses come to an end when iron is formed in their core. Iron absorbs energy and does not fuse into heavier elements, it also does not release energy by fission. Thus, the inward pull of gravity overcomes the outward thermal pressure and the star collapses in on itself. At the core of the collapsing star the force of gravity overcomes electron degeneracy pressure and protons and electrons come together to form neutrons, over-riding the weak nuclear force. Due to conservation laws, neutrinos are released during this process causing the core to cool and compress even more until the inner core reaches nuclear density. At this point the strong nuclear force, which is the force that keeps the nuclei of atoms together against the repulsive force between neutrons, takes over and causes the core to bounce, as if a wall was formed at the interior, creating a shock wave which travels out through the in-falling outer core. If the shock wave stalls, collapse continues, overriding the strong nuclear force, and a black hole is formed. However, it is possible that the shock wave is regenerated by some underlying mechanism which heats up the star and produces new elements. If this occurs, or the shock wave is not stalled and reaches the surface, the star explodes in a supernova leaving either a black hole or neutron star.

The mechanism causing shock wave revival is debated by theorists. The two front-running theories are the *neutrino mechanism* and the *magnetorotational mechanism.*[Bethe and Wilson, 1985], [Shibata et al., 2006] The neutrino mechanism is based on the idea that high-energy neutrinos are trapped behind the stalled shock wave and that they somehow regenerate it. The magnetorotational mechanism suggests that the shock wave is regenerated by strong differential rotation in the outer protoneutron star.

2.2 Statistical Methods

2.2.1 Principal Component Analysis

Principal component analysis is a multivariate dimension reduction technique that transforms a set of potentially correlated variables into a set of orthogonal principal components. As described in Rencher and Christensen, given some data, the aim of principal component analysis is to sequentially maximize the variance of an orthogonal combination of the variables.[Rencher and Christensen, 2002] The first principal component is the linear combination with maximal variance; the dimension along which the observations are maximally

separated or spread out. The second principal component is the linear combination with maximal variance in a direction orthogonal to the first principal component, and so on.

Principal components have a simple geometric intuition. Principal component analysis deals with a sample of n observation vectors each of length p $\boldsymbol{y}_1, \boldsymbol{y}_2, \ldots \boldsymbol{y}_n$. These observations form a swarm of points in p-dimensional space. For simplicity, although it is not required for principal component analysis, it helps to visualize this swarm as ellipsoidal. If the observations are correlated, the ellipsoidal swarm will not be oriented along the axes represented by $y_1, y_2, \ldots, y_p$. Our goal is to find the natural axes of the ellipsoid with origin located at $\bar{\boldsymbol{y}}$. This is done by translating the origin to $\bar{\boldsymbol{y}}$ and rotating the axes. Once the axes are rotated to be along the natural axes of the ellipsoid, the new variables (principal components) will be orthogonal and therefore uncorrelated. This can be done by finding the eigenvectors of the covariance matrix of the data.

Following the presentation in Heng 2009, and keeping with the context of this paper, we arrange the waveforms from the catalog $\{H_1, H_2, \ldots, H_M\}$ into a matrix such that each column corresponds to one of the waveforms.[Heng, 2009] For M waveforms of length N, the matrix $\mathbf{H}$ has dimensions $N \times M$. First, Ψ, a matrix of mean-subtracted waveforms is constructed such that the columns, Ψ_i, are determined by.

$$\Psi_i = H_i - \frac{1}{M} \sum_{i=1}^{M} H_i$$

The covariance matrix is then calculated by

$$\boldsymbol{C} = \frac{1}{M} \Psi \Psi^T$$

where $\mathbf{C}$ is the covariance matrix with dimensions $N \times N$.

The normalized eigenvectors of $\mathbf{C}$ form a basis set of vectors that span the parameter space defined by the waveforms in $\mathbf{H}$. The eigenvalues of the covariance matrix, λ_i, indicate how well their corresponding eigenvector spans the space of the waveform catalog. They are constructed so that a proportion, $\sum_{i=1}^{k} \lambda_i^2 / \sum_{i=1}^{M} \lambda_i$, of the total variation of the waveforms is explained by the selected k eigenvectors. See figure **??** below for a visual representation of these normalized eigenvalues.

2.2.2 Principal Component Regression

Principal Component Regression (PCR) is a linear regression with the principal component basis vectors treated as explanatory variables. Dimension is reduced by only considering the

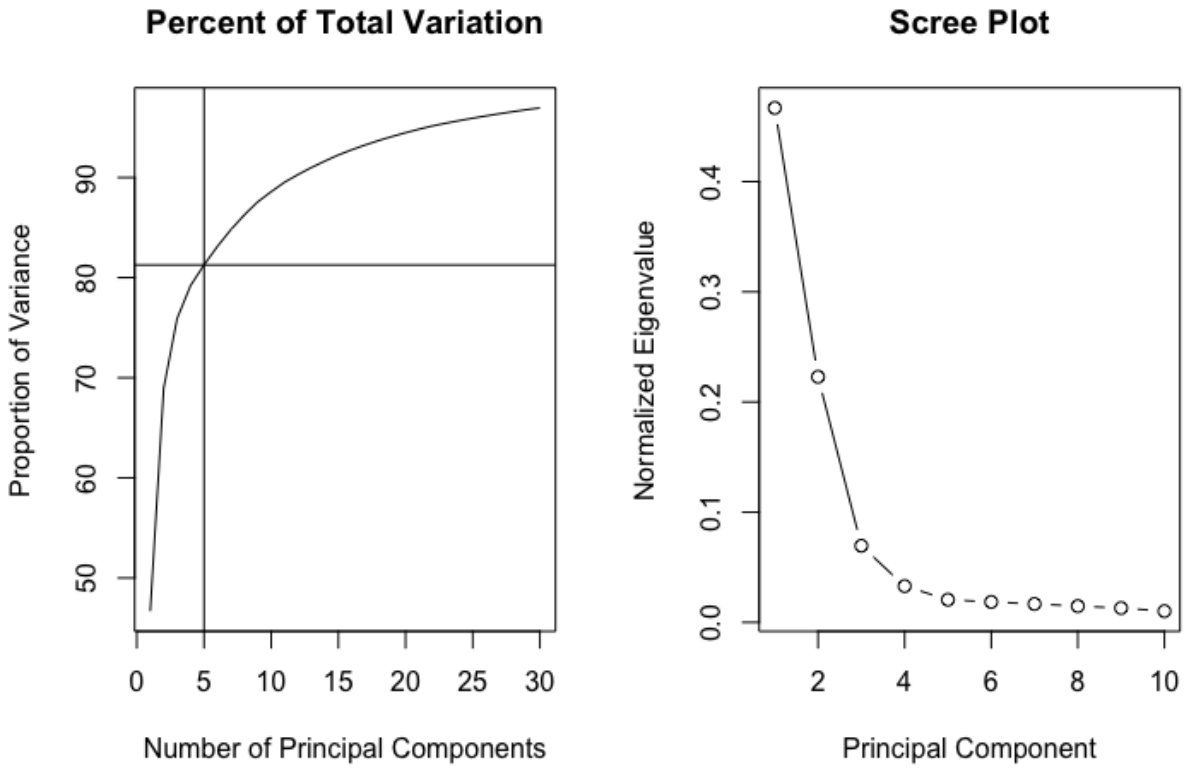

Figure 1: Common graphical methods for selecting number of principal components. Created using 136 simulated Core Collapse Supernova Signals from Dimmelmeier et al. [Dimmelmeier et al., 2008]

first d basis vectors with the highest eigenvalues, which conserve as much of the information about the original data as possible. Choosing the number of basis vectors to retain is a non-trivial problem. This is generally done heuristically although cross-validation methods may also be employed. Rencher and Christensen propose the following guidelines for selecting the number of principal components to retain.[Rencher and Christensen, 2002]

1. Retain sufficient components to account for a specified percentage of the total variance, say 80%. An example of this decision criterion being used to select a number of principal components for the Dimmelmeier et al waveform catalog is displayed in Figure 1.[Dimmelmeier et al., 2008]

2. Retain the components whose eigenvalues are greater that the average of the eigenvalues, $\sum_{i=1}^{p} \lambda_i/p$. For a correlation matrix, this average is 1.

3. Use the *scree graph*, a plot of λ_1, verses i, and look for a natural break between the

"large" eigenvalues and the "small" eigenvalues. An example of a scree graph for the same Dimmelmeier et al. waveform catalog is displayed in Figure 1

4. Test the significance of the "larger" components, that is, the components corresponding to the larger eigenvalues using a liklihood ratio test.

2.2.3 Time Series

Gravitational waves are finite duration discrete time series. An important simplifying assumption of the analysis done is that the time series are stationary. The basic idea of stationarity is that the probability laws that govern the behavior of the process do not change over time. Mathematically, a weakly stationary time series $\{X_t\}$ has constant and finite mean and variance over time, and an autocovariance function $\gamma(t, t-h) = Cov(X_t, X_{t-h})$ that depends only on the time lag h. Thus, a time series is second order stationary if

$$E[X_t] = \mu < \infty, \quad \text{for all time } t$$

$$Var[X_t] = \sigma^2 < \infty, \quad \text{for all time } t$$

$$\gamma(t, t-h) = \gamma(0, h), \quad \text{for all time } t \text{ and lag } h$$

Stationary time series are often modeled using the autoregressive moving average (ARMA) model. As its name suggests, the ARMA model is made up of two parts: an autoregressive component and a moving average component. Assuming a mean-centered time series $\{X_t\}$, an ARMA(p, q) model is formulated as follows,

$$X_t - \sum_{i=1}^{p} \phi_i X_{t-i} = \epsilon_t + \sum_{t=1}^{q} \theta_i \epsilon_{t-1}$$

where p is the number of autoregressive terms, q is the number of moving average terms and ϵ_t is white noise with zero mean and constant variance. If $p = 0$, the ARMA model reduces to a moving average (MA) model of order q . If $q = 0$, it reduces to an autoregressive (AR) model of order p. If $p = q = 0$, the model reduces to white noise.

2.2.4 Fourier Transform

The Fourier transform maps a function of time to a function of frequency using complex sinusoids. The Fourier transform is immensly useful in time series analysis because many problems are naturally solved in the frequency domain instead of the time domain. Formally, following the presentation in Edwards let $h : \mathbb{R} \to \mathbb{R}$ be a continuous real valued time series,

then it's continuous Fourier transform $\tilde{h} : \mathbb{R} \to \mathbb{C}$ is the continuous complex-valued function defined as

$$\tilde{h}(\lambda) = \int_{-\infty}^{\infty} h(t) e^{-i\lambda t} dt$$

where $\lambda = 2\pi\nu$ is angular frequency with ν measured in cycles per unit time.[Edwards, 2017]

The operation that reverses the transformation is called the continuous inverse Fourier transform, and is defined as

$$h(t) = \frac{1}{2\pi} \int_{-\infty}^{\infty} \tilde{h}(\lambda) e^{i\lambda t} d\lambda$$

The Fourier transform and its inverse may be thought of as a Fourier transform pair, given by

$$h(t) \rightleftharpoons \tilde{h}(\lambda)$$

2.2.5 Properties of the Fourier Transform

Because h is a real-valued function, the inverse transform $\tilde{h}$ is Hermitian symmetric.

$$\tilde{h}(-\lambda) = \overline{\tilde{h}(\lambda)}$$

where $\overline{\tilde{h}(\lambda)}$ is the complex conjugate of $\tilde{h}(\lambda)$.

The Fourier transform is linear. Let $h(t) \rightleftharpoons \tilde{h}(\lambda)$ and $g(t) \rightleftharpoons \tilde{g}(\lambda)$ be Fourier transform pairs, then

$$ah(t) + bg(t) \rightleftharpoons a\tilde{\lambda} + b\tilde{g}(\lambda),$$

for any real numbers a and b By the convolution theorem, a convolution in the time domain forms a Fourier transform pair with multiplication in the frequency domain. That is, the inverse Fourier transform of the product of two continuous Fourier transformed series is their convolution. Mathematically,

$$h(t) * g(t) \rightleftharpoons \tilde{h}(\lambda)\tilde{g}(\lambda)$$

where

$$h(t) * g(t) = \int_{-\infty}^{\infty} h(t - \tau) g(\tau) d\tau$$

is the convolution of h and g. The same is true in reverse. Multiplication in the time domain forms a Fourier transform pair with a convolution in the frequency domain. The Fourier transform has the following time-shifting property,

$$h(t - T) \rightleftharpoons e^{-i\lambda T}\tilde{h}(\lambda),$$

for any time lag T. That is, shifting a time series h by lag T can be done in the frequency domain by multiplying the Fourier transform of the series by $e^{-i\lambda t}$.

2.2.6 Discrete Fourier Transform

The discrete Fourier transform (DFT) converts a finite sequence of discrete time values to a finite set of Fourier coefficients in the frequency domain. Formally, following the presentation in Rowe 2016, the one dimensional discrete Fourier transform $F(q\Delta v)$ of a time series $y(t)$ sampled at N times Δt apart is defined as,

$$f(q\Delta\nu) = \sum_{p=1}^{N} y(p\Delta t)e^{-i2\pi(p-1)(q-1)/N}$$

for $p, q = 1, \ldots, N$, and $\Delta\nu = 1/(N\Delta t)$.[Rowe, 2016] Like the continuous Fourier transform, the DFT is made up of both real and imaginary parts. The DFT and inverse DFT are efficiently computed using the fast Fourier transform (FFT).[Cooley and Tukey, 1965] Like the Fourier transform, the DFT also has Hermitian symmetry if h is real-valued. If N is even, then there are $\frac{N}{2} + 1$ non-redundant DFT elements. Also, $\tilde{h}(0)$ and $\tilde{h}(\frac{N}{2}\lambda)$ are always real valued. This means that there are $\frac{N}{2} + 1$ real parts and $\frac{N}{2} - 1$ imaginary parts.

2.2.7 Template Matching

Template matching is a technique used in signal and image processing for locating small parts in an image that match a given template. Facial recognition is a common problem that relies on template matching. Template matching based on feature extraction methods is often performed using Neural Networks and Deep Learning classifiers but at its core it is a simple approach which can be applied rapidly and with computational efficiency.

A simple approach to template matching is to calculate the correlation between the template and the signal or image. This calculation is then repeated, moving the template over each pixel or lag value in the signal. This process returns a series or matrix of correlations between template and signal which is the same size as the signal. In the context of this paper we are examining time series which are encoded as 1-dimensional vectors. The mathematics will be presented in these terms.

Let X and Y be two time series of equal length n. Recall Pearson's Correlation coefficient,

$$Corr[X, Y] = \frac{Cov[X, Y]}{\sqrt{Var[X]Var[Y]}}$$

assuming that the two time series are mean centered this becomes,

$$Corr[X, Y] = \frac{E[XY]}{\sqrt{Var[X]Var[Y]}} = \frac{\frac{1}{n}Sxy}{\sqrt{Var[X]Var[Y]}}$$

where,

$$Sxy = \frac{1}{n-1}\sum_{i=1}^{n}(x_i - \bar{x})(y_i - \bar{y})$$

The two variances in the denominator are easily calculated for discrete time series. Calculation of the numerator can be done using the convolution theorem discussed in section 2.2.4 above as,

$$Sxy = \mathcal{F}^{-1}[\mathcal{F}[X]\overline{\mathcal{F}[Y]}]$$

Where, $\mathcal{F}$ is the Fourier transform. Thus we have that,

$$Corr[X,Y] = \frac{\frac{1}{n}\mathcal{F}^{-1}[\mathcal{F}[X]\overline{\mathcal{F}[Y]}]}{\sqrt{Var[X]Var[Y]}}$$

Remark: Note that $\mathcal{F}^{-1}[\mathcal{F}[X]\overline{\mathcal{F}[Y]}]$ is commonly referred to as the cross-correlation in signal processing. Formulating the problem in this way allows us to use the FFT which significantly speeds up calculations. Additionally, performing these calculations in the frequency domain allows all correlations to be calculated at once. Instead of calculating n individual correlations at each lag, all correlations are calculated at once with the cross-correlation.

2.2.8 Interpolating Splines

Interpolation between measured points is a common problem in time series analysis. For a time series of length n it is infeasable to interpolate using a polynomial of degree n, which, while it will perfectly fit all n points, will be poorly conditioned and highly variable to small changes in the input. Instead of globally overfitting the data it is possible to fit a piecewise polynomial function, known as a spline, formed by $n-1$ low degree polynomials. This polynomial can be additionally constrained by requiring its derivatives to exist so that it must be continuous and smooth.

Let $S(x)$ be a piecewise polynomial spline and let $P_i(x)$ be the i^{th} polynomial piece of $S(x)$. Then, for $S(x)$ to be continuous we must have,

$$P_i(x_i) = P_{i+1}(x_i) = y_i$$

for each i, or that each consecutive polynomial is joined with the previous one at their endpoint. For $S(x)$ to be smooth the consecutive polynomials must have the same derivative at their joint. Thus,

$$P_i^{(k)}(x_i) = P_{i+1}^{(k)}(x_i)$$

must hold for some order k. The spline becomes more smooth for higher values of k.

Cubic Splines, where the piecewise polynomials are third order, provide a good middle ground between flexibility and overfitting. Cubic splines also have the benefit of being easy to obtain. Requiring that the second derivative of each polynomial is zero at their endpoints provides a boundary condition which leads to a tridiagonal system which can be easily solved for the polynomial coefficients. This is known as the "natural" cubic spline.

3 Analysis

3.1 Outline

The analysis performed for this paper followed these steps.

1. The waveforms created by Abdikamalov et al. were smoothed and resampled at the LIGO sampling rate 2^{14} Hz.

2. The waveforms were injected into noisy samples of length 2^{15} with signal-to-noise ratios (SNRs) 10 and 20

3. Locations of interest were selected out of the noisy data stream using template matching, where the signals in training set from the waveform catalog were used as templates.

4. Using PCR, the locations of interest were reconstructed and coefficients for the original test catalog were found for each.

5. Hypothesis tests on the significance of the test signals were applied.

3.2 Waveform Catalog

The gravitational wave waveforms used in this analysis come from two-dimensional numerical axisymmetric general-relativistic hydrodynamic rotating core collapse and bounce surpernova simulations.[Abdikamalov et al., 2014] A single presupernova progenitor model (the 12 solar mass at zero age main sequence solar-metallicity progenitor model from Woosley and Heger was assumed. It has been shown that gravitational wave signals from core collapse supernova are essentially independent of the zero age main sequence of the progenitor star.[Woosley and Heger, 2007]

The waveform catalog was partitioned into training and test sets. The training set contains 92 signals with varying parameters. The training set is partitioned by five levels of precollapse differential rotation A where higher levels of A correspond with weaker differential rotation. At each level A, simulations were run over a grid of values for initial central angular velocity Ω_c, and then for a grid of values for the ratio of rotational kinetic energy of gravitational energy of the inner core at bounce $\beta_{ic,b}$. Each signal in the training set was generated using the microphysical Lattimer-Swesty (LS) equation of state (EOS) [Lattimer and Swesty, 1991], the parametrized deleptonization scheme from

[Dimmelmeier et al., 2008], and the neutrino leakage scheme from [Ott et al., 2012]. In addition to varying underlying values of A, Ω_c, and $\beta_{ic,b}$, the test set contains 47 signals with differing EOS and deleptonization parametrizations. Specifically, some of the signals in the test catalog were created using the Shen EOS [Shen et al., 1998] and by increasing/decreasing the deleptonization parametrization by $\sim 5\%$. The values of Ω_c and $\beta_{ic,b}$ in the test set were generated over a different grid, but in the same parameter space as the training set. The object of our analysis is to to detect and reconstruct waveforms from the test set embedded in simulated detector noise and infer their physical parameters.

Preparing the signals in the catalog for analysis required them to be resampled. The signals were initially sampled at 100 kHz and were downsampled to 16384 Hz (the sampling rate of the Advanced LIGO detectors) using cubic spline interpolation. The resampled data was then zero-buffered to insure that each signal was the same length, $n = 16384$, corresponding to a length of 1 s of data collected by Advanced LIGO. The waveforms are all initially of mean zero, so zero-buffering has no effect on the overall mean. After this, each signal was aligned so that their minima, which corresponds to the location of the core bounce, was located at the center of the time series. This follows the setup of [Röver et al., 2009] In this analysis, the source of a gravitational wave emission is assumed to be oriented perpendicular to a single interferometer. Each signal is linearly polarized with zero cross-polarization.

The general shape of the waveforms are displayed in Figure 2. During core collapse, there is a slow increase in gravitational wave strain until the first local maximum is reached. Then there is an abrupt decrease toward a local minima, located at 0.5 s, at core bounce. The minimum achieved corresponds with the expansion of the inner core during bounce. Following this is a period of ring down oscillations as the proto-neutron star core settles. Immediately noticeable is the variability in magnitude of the initial drop and following peak. These differences are driven by the initial differential rotation of the progenitor star. For slowly rotating progenitor stars, $\beta_{ic,b} \sim 0.03$, the pre- and post-bounce peaks are of similar size and the minimum at bounce is relatively small, an example of which is displayed in the second panel above. For rapidly rotating progenitors, $\beta_{ic,b} \sim 0.09$, like those displayed in the first and third panel above, The pre-bounce maximum is much smaller than the post-bounce maximum, and the intermediate minimum is greater in magnitude than for slowly rotating progenitors.

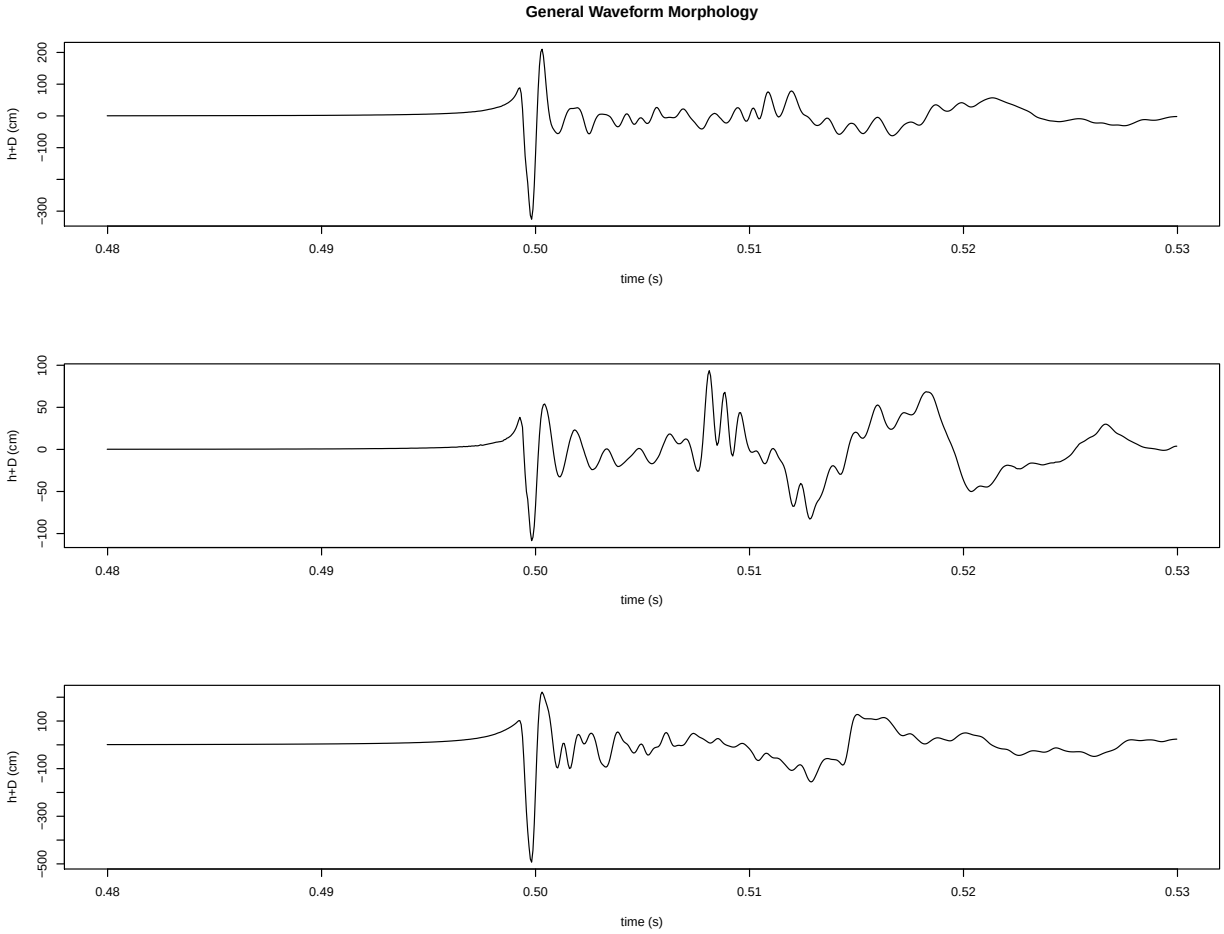

Figure 2: General waveform morphology for Abdikamalov et al. Catalog

3.3 Principal Component Analysis

To reduce dimension, principal component analysis was applied to the base catalog of waveforms. Each training waveform is represented as a linear combination of orthonormal basis vectors. The projection of the data onto the first basis vector has maximal variance, the projection on to the second basis vector has the second highest variance, and so on. By considering only the projections onto a beginning subset of the 92 basis vectors, a parsimonious representations of the signals that preserves as much information as possible is achieved. The first four principal components of the base catalog are depicted in Figure 3. [Note that the first two PCs captures the essential pre- and post-bounce maxima on a large scale, whereas the later PCs capture the post-bounce variation that is common in all waveforms in the catalog.] In this analysis, PCA was performed by taking the singular value decomposition (SVD) of the base catalog using the base R SVD command. This approach was significantly

faster than computing the spectral decomposition of the catalog. It also allows for easy reconstruction of a reweighted waveform matrix by saving the right singular vectors V for right multiplication after principal component regression (PCR) is performed.

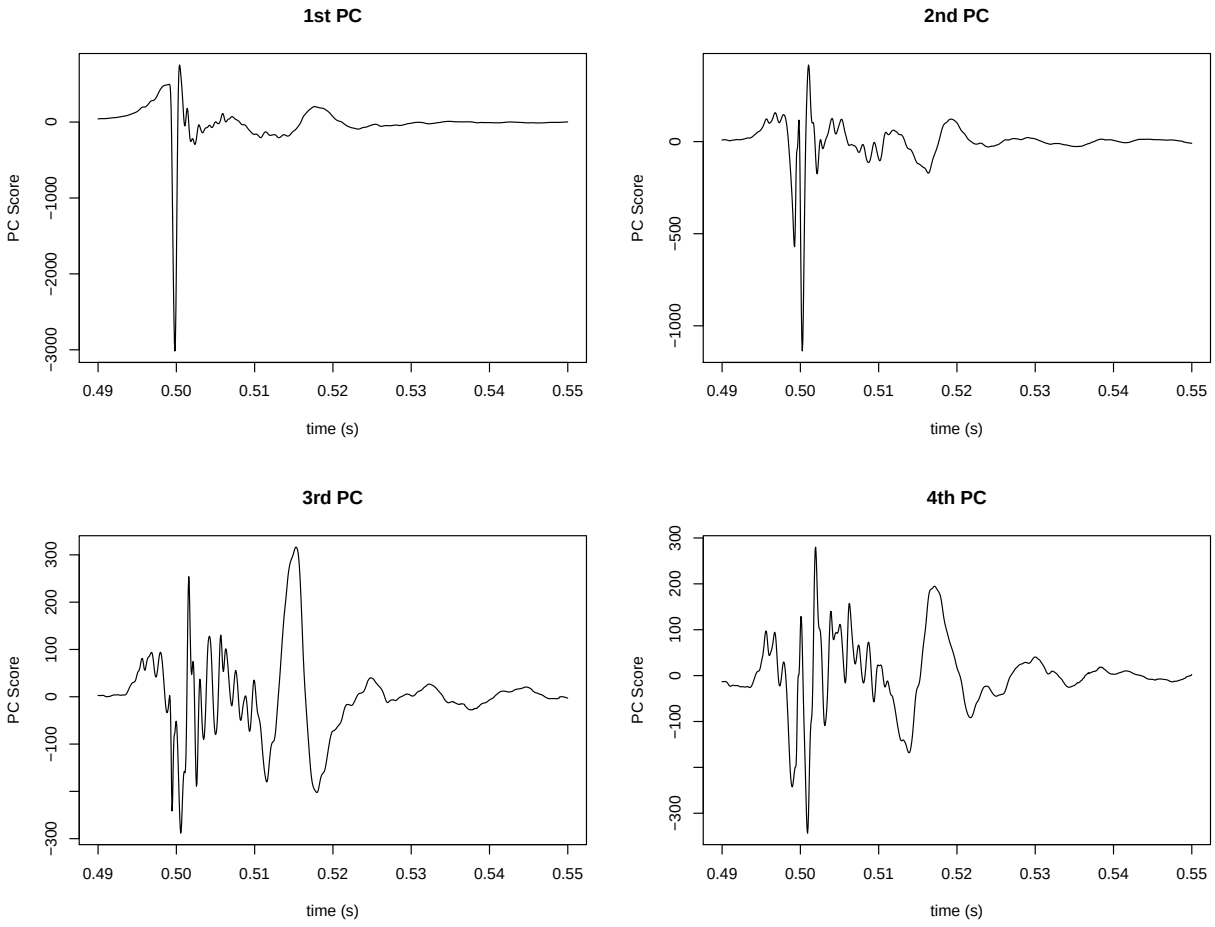

Figure 3: First Four Principal Components

3.4 Simulation of Gravitational Wave Data

Data obtained by Advanced LIGO is contaminated with noise covering the entire range of the detectors bandwidth. The detectors are incredibly sensitive, as they must be, and measure noiseplo from many sources. From shot noise in photon intensity readings and impurities in the reflective mirrors, to terrestrial noise from trucks passing nearby on the highway or, reportedly for the detector in Washington, from waves crashing on the shores of California.[Abbott et al., 2016a] The detection frequency band for Advanced LIGO covers the whole gamut of noise sources including seismic, thermal and quantum noise. Accurate astrophysical inference relies on an honest characterization of background and detector noise sources. As such, proper statistical reconstruction of detector noise is an open and active area of research for the gravitational wave community.

A common assumption in gravitational wave data analysis is that the noise is essentially stationary and Gaussian distributed, with a known phase spectral density (PSD) that can be estimated using off-source signal. Unfortunately, this has been shown to be false.[Cornish and Littenberg, 2015] Non-Gaussian glitches due to terrestrial disturbances pervade the data stream, and the noise exhibits behavior of a fatter tailed than Gaussian process. These inconsistencies with assumption can lead to misleading inferences and predictions about underlying signal. To capture this non-Gaussian behavior, noise is modeled as an autoregressive (AR) process with Student-t innovations with $\nu_{df} = 3$ degrees of freedom. The effect of using Student-t innovations with $\nu_{df} = 3$ is the introduction of transient, high-amplitude, non-Gaussian events. These are a result of the fat-tailed nature of the Student-t density which is amplified by the choice of $\nu_{df} = 3$ which is the lowest degrees of freedom for which the Student-t density has non-infinite variance. This choice of noise model reasonably matches the PSD of the LIGO data stream as well as being easily generated.

To generate signals with a given Signal-to-Noise Ratio (SNR) the following process is applied. Add together a signal from the waveform catalog and some generated noise process such that the sum has the desired SNR. SNR may be defined as,

$$SNR = \frac{\mu}{\sigma}$$

using this definition we may generate signals with desired SNR. The resampled signals in the waveform catalogs have mean zero. By adding 100 to each element in the time series the mean is moved to $\mu = 100$. This allows us vary σ to obtain non-zero SNR. The AR1(-0.9) process is stationary, so it is generated with constant mean $\mu_{noise} = 0$ and $\sigma^2_{noise} = \sqrt{\frac{3}{1-(-0.9)^2}}$.

Using these pieces we calculate the value of the constant $c = \frac{\mu}{\sigma_{noise} SNR}$ that when multiplied by the original noise time series shifts it such that the sum of the original waveform and the new noise have the desired SNR. Figure 4 displays an identical true waveform in red encased in noise with SNR values 20 and 10.

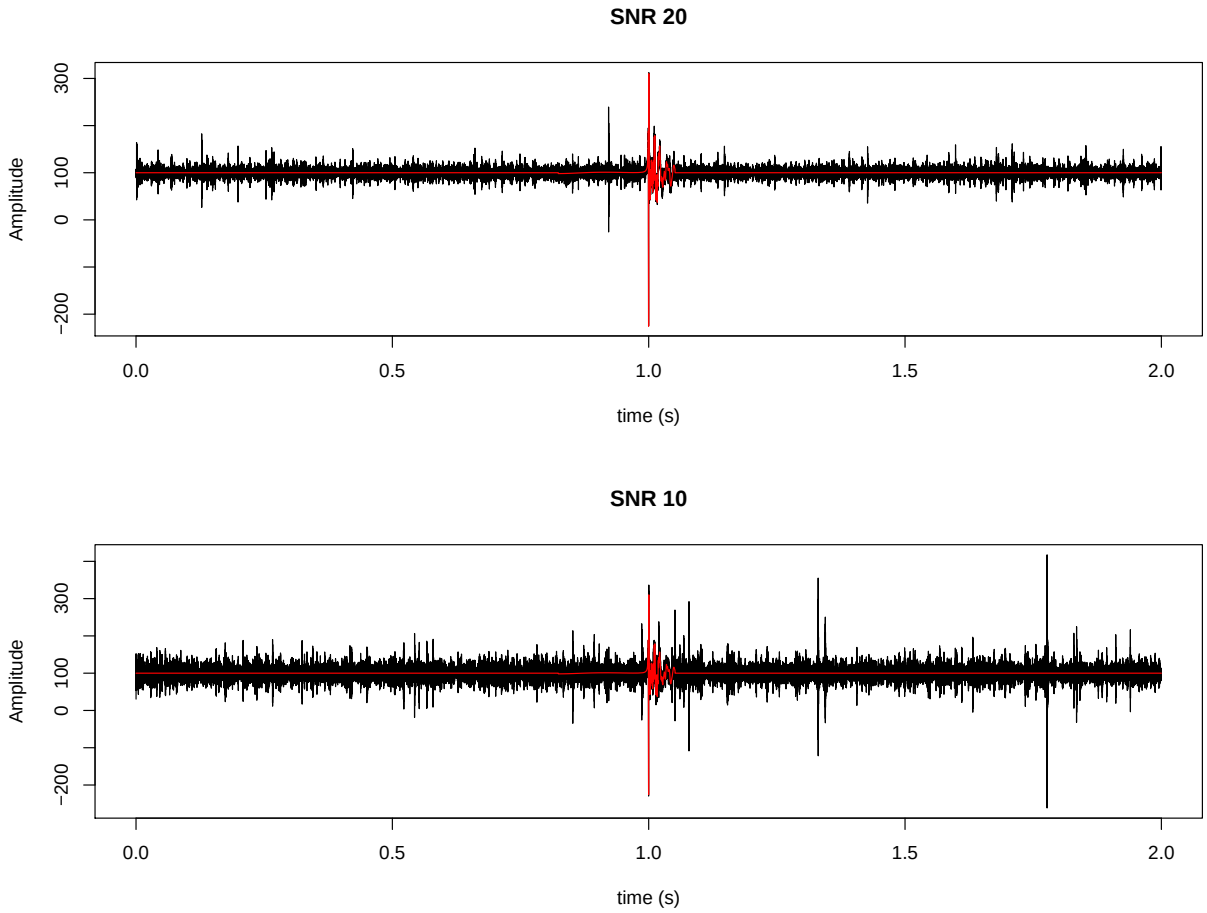

Figure 4: Identical waveform injected into sample with SNR 20 and 10

Data is simulated at both both SNR 10 and 20 for each waveform in both the base and test catalogs. In total 278 simulated signals were created. For simplicity, each of these signals were injected with waveforms around the center of the time series. voided problems with wrap-around and allowed for easy verification of correct detection.

3.5 Template Matching

The problem of detecting signals in a noisy sample can be solved in many ways. One method used by LIGO scientists is cross-correlation of sections of the data stream taken

at the same time from the Livingston and Hanford detectors. Assuming independent noise sources, which is generally true, excluding tectonic noise, high cross-correlation indicates that the same signal was detected by both interferometers at the same time, differing only by the time it takes light to travel from Washington to Louisiana ($\sim$ 10 ms), which would be a likely candidate for an astrophysical event. For inspiral gravitational wave signals detection and inference are performed at the same time using template matching. In the case of black hole-black hole binaries, only four parameters, the mass and spin of the two black holes, are needed to cover the parameter space of events. Thus, it is possible to test a catalog of templates which sufficiently spans the parameter space against the signal which, in the case of detection, also parametrizes the source all very quickly due to use of the FFT. Generally, for burst signals template matching is not used because the signals are poorly modeled, or the sources are entirely unknown. For signal from core collapse supernovae, inference using template matching is impossible due to the high dimension of the parameter space. It would be computationally infeasible to run enough simulations to obtain templates which even moderately cover this space. This does not mean that template matching is useless, as due to the similarity in general waveform morphology, it can still be used to help with detection of likely candidates in the data stream.

The detection criterion used in template matching is Pearson's correlation coefficient ρ which is a simple measure of linear dependence between two random values or random vectors. The correlation, ρ, is a unitless quantity which takes on values, $-1 \leq \rho \leq 1$, where -1 indicates perfect negative linear dependence and 1 indicates perfect positive linear dependence. Calculation of the correlation between a template time series from the waveform catalog and a simulated signal for each pixel in the signal can be performed quickly using the Fast Fourier Transform (FFT) as discussed in section 2.2.7 above. Figure 5 displays the results of this computation for one template-signal pair. The top panel shows the correlation time series whose elements are the correlations between the signal in the bottom panel and the template, displayed in the middle panel, centered on that time. This process can be imagined as overlapping the Template and Signal panels, calculating the correlation and storing it, sliding the template one time-step while holding the signal in place and calculating a the new correlation, and so on. Again and again until cross-correlation has been calculated at all time steps

Figure 5 displays the correlation between the template corresponding to the first waveform in the catalog, and a simulated signal with SNR = 10 generated using the same wave-

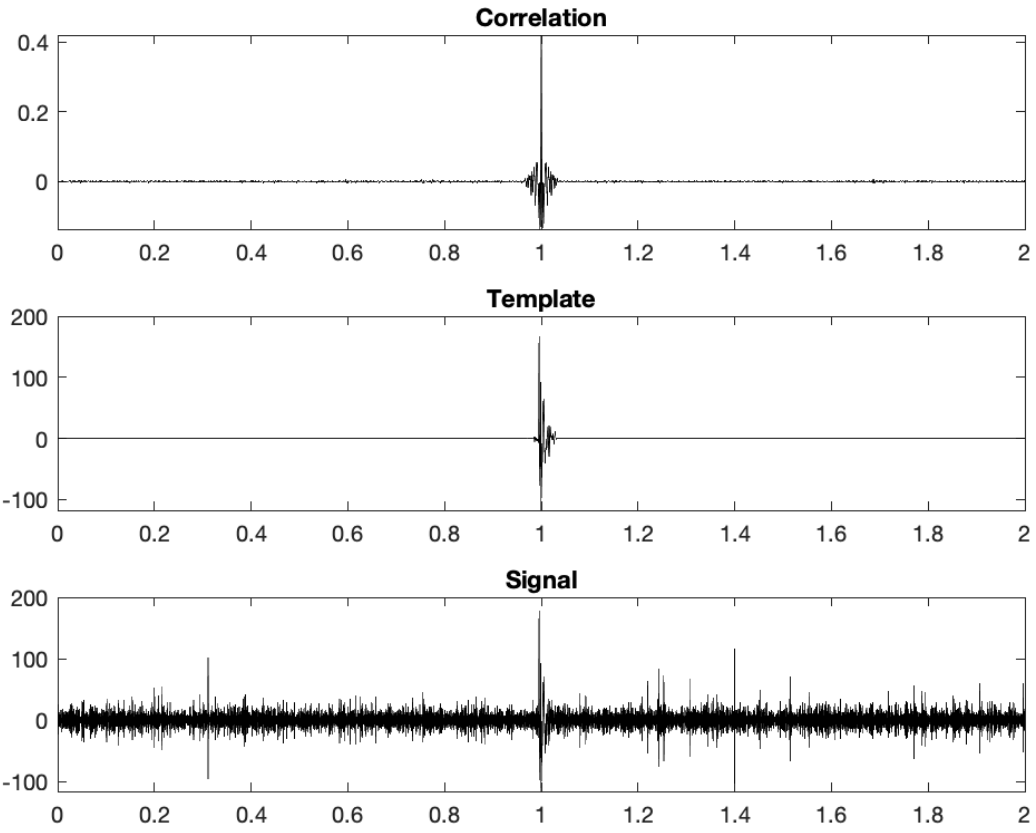

Figure 5: Correlation between Template and Simulated Signal

form. It is not always the case that the template which obtains a high correlation and the underlying waveform injected into the signal match. Additionally, setting the threshold for what is considered a "high" correlation at too large a value increases the number of false negatives or failures to correctly detect a signal. Thus, it is important to have some statistical criteria for choosing a threshold.

One such criterion is to find the critical values for correlation between two time series at which we have confidence that the similarity between the two signals cannot be due to random fluctuation. Following the appendix in Rowe 2003 we find that the 0.1% critical value for correlation between two random time series with 200 degrees of freedom is 0.2183.[Rowe et al., 2003] The degrees of freedom of the waveforms in this analysis is $2^{14} = 16384$. This is much greater than 200, and consequently, the 0.1% critical value will be smaller still than the already low correlation value required for a highly confident match in the smaller sample case. Figure 6 displays the distributions of correlations for all template

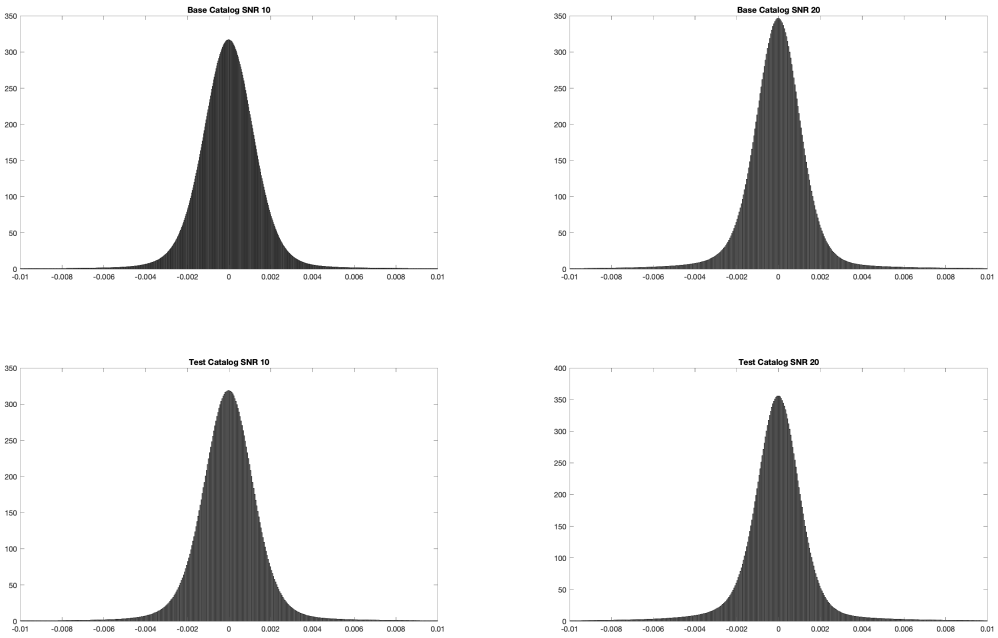

Figure 6: Histograms of Correlations between Templates and Waveforms

matching runs on each of the signal catalogs. Figure 6 gives some indication of the rarity of high correlation values.

Core collapse supernova are extremely rare events. The expected number of events in the Milky Way Galaxy is on the of order one per century. Thus it is important that no potential signals are overlooked. Stated differently, in this analysis, false negatives are much worse than false positives. Setting the correlation threshold value at 0.3 led to many false negatives. All but a small number of the waveforms were left with no matches. Lowering the threshold to 0.21 and 0.1 ameliorated the problem of false negatives and but introduced false positives. Figure 7 displays an example from the test catalog of signals where a template which did not match the underlying waveform was counted as a match.

After performing template matching using all combinations of templates and signals and selecting a correlation threshold, locations of interest in each signal were selected and recorded. The one second pieces of the signals indicated by these addresses of locations of interest are then analyzed using a principal component regression and a reconstruction of the underlying waveform is generated.

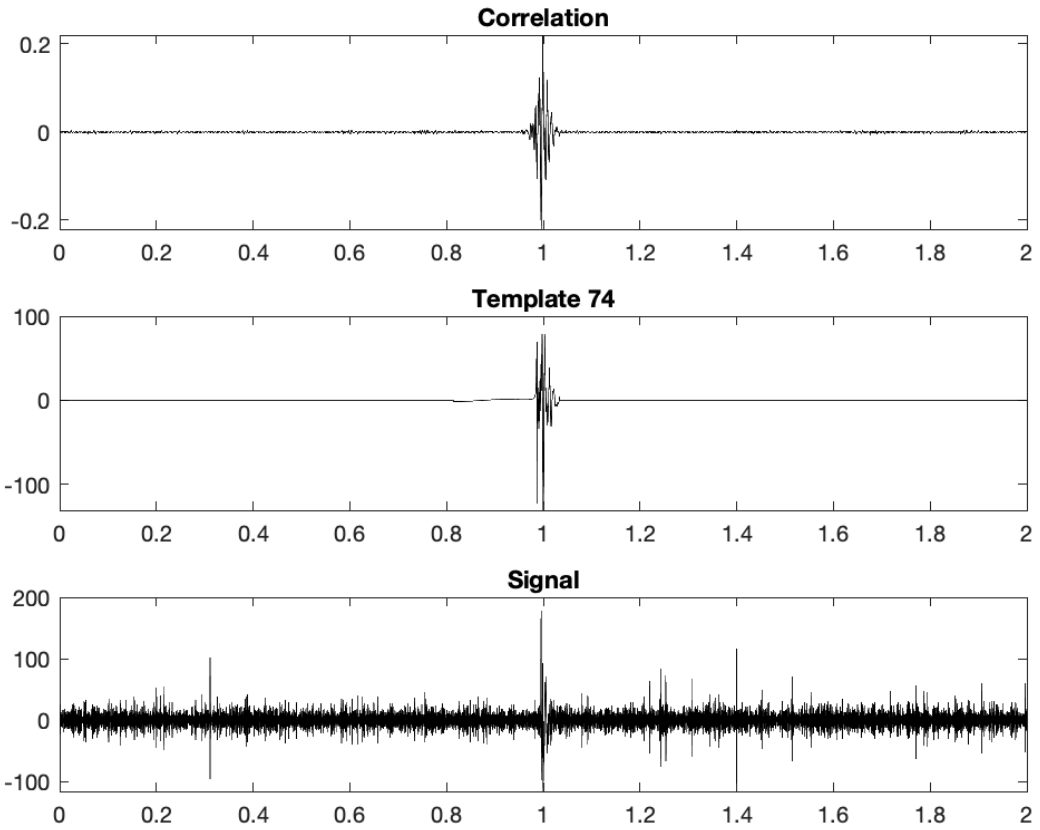

Figure 7: Positive result for $\rho_{\text{threshold}} = 0.2183$ where the template and underlying waveform do not match.

3.6 Signal Reconstruction

As discussed in Section 2.2.2 above, an important step in running a PCR is to select a reasonable number of principal components. Using all 92 principal components obtained from the base catalog as regressors would defeat their stated purpose, to reduce dimension. Following the suggestions in Rencher and Christensen the plots displayed in Figure 8 were constructed and analyzed.[Rencher and Christensen, 2002] The scree plot in the right panel is not helpful with regard to selecting the number of components. The elbow-like bend occuring between components number two and three is indicates that the first component does the best job of explaining the variability in the catalog by a wide margin. Returning to Figure 3 we see that the first principal component captures the pre- and post- bounce maxima, and the large negative peak at bounce. This matches with our intuition as it is the essential behavior visible in all of the waveforms as shown in Figure 2.

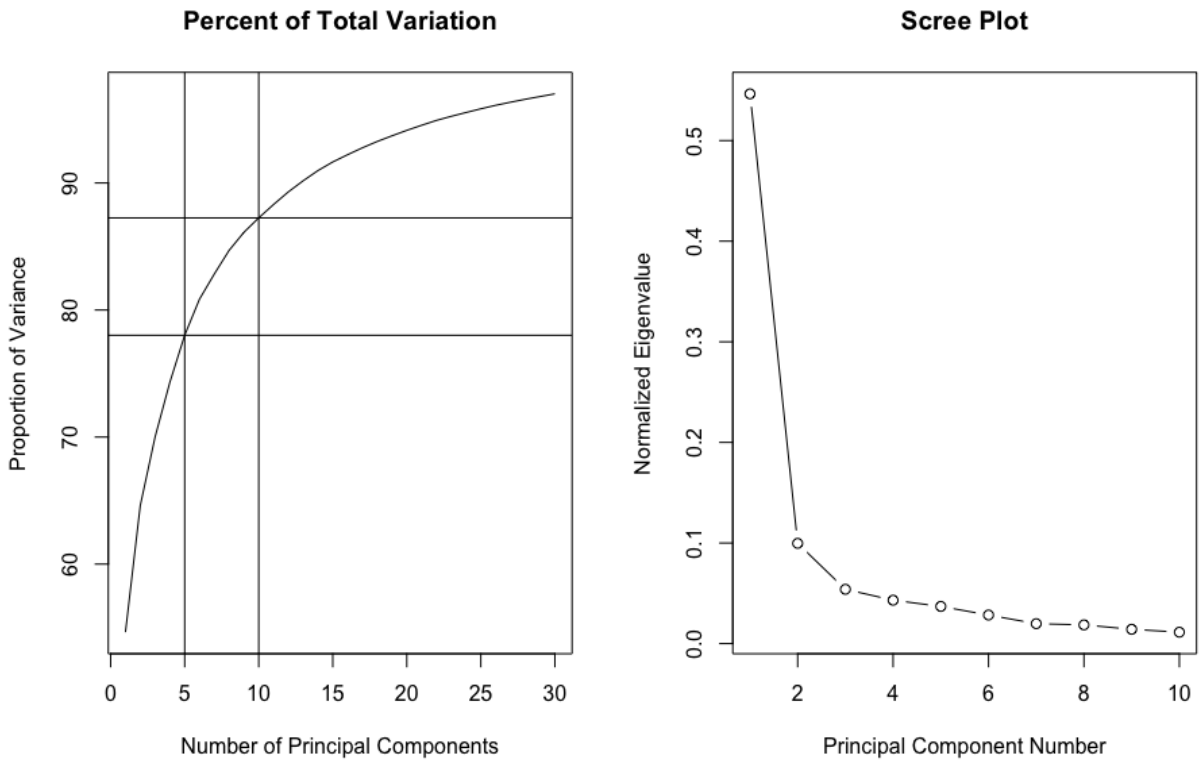

Figure 8: Graphical Methods used to help selecting number of Principal Components

The left plot in Figure 8 is more useful for our purpose. By only considering 10 of the 92 principal components almost 90% of the variability in the data is explained. The exact values for the two proportions of variance when 5 and 10 principal components are considered are 78% and 87.25% respectively. After examining these plots the decision was made to use 10 principal components in the regression. This is slightly lower than the number of principal components shown by Edwards to minimize the deviance information criterion, a generalization of the Akaike information criterion useful in Bayesian model selection, while minimizing the number of components. Once a number of components was chosen, regression was performed as follows.[Edwards, 2017]

Let W be the matrix of principal components arranged as columns and let y_i be the vector of length 2^{14} corresponding to the i^{th} match indicated by template matching. The vector of regression coefficients $\hat{\gamma}_i$ is obtained in the usual way by,

$$\hat{\gamma}_i = (W^T W)^{-1} W^T y_i,$$

Using these coefficients we obtain an estimate $\hat{y}_i$ of the underlying signal by,

$$\hat{y}_i = W\hat{\gamma}_i.$$

One such reconstruction is displayed in figure 9. This process can be performed for all $\hat{y}_i$ at once. Let Y be a matrix with columns y_i. Then, $\hat{\Gamma}$ the matrix with $\hat{\gamma}_i$ as columns is obtained by,

$$\hat{\Gamma} = (W^T W)^{-1} W^T Y$$

in this way, reconstructions of all of the matched signals were obtained.

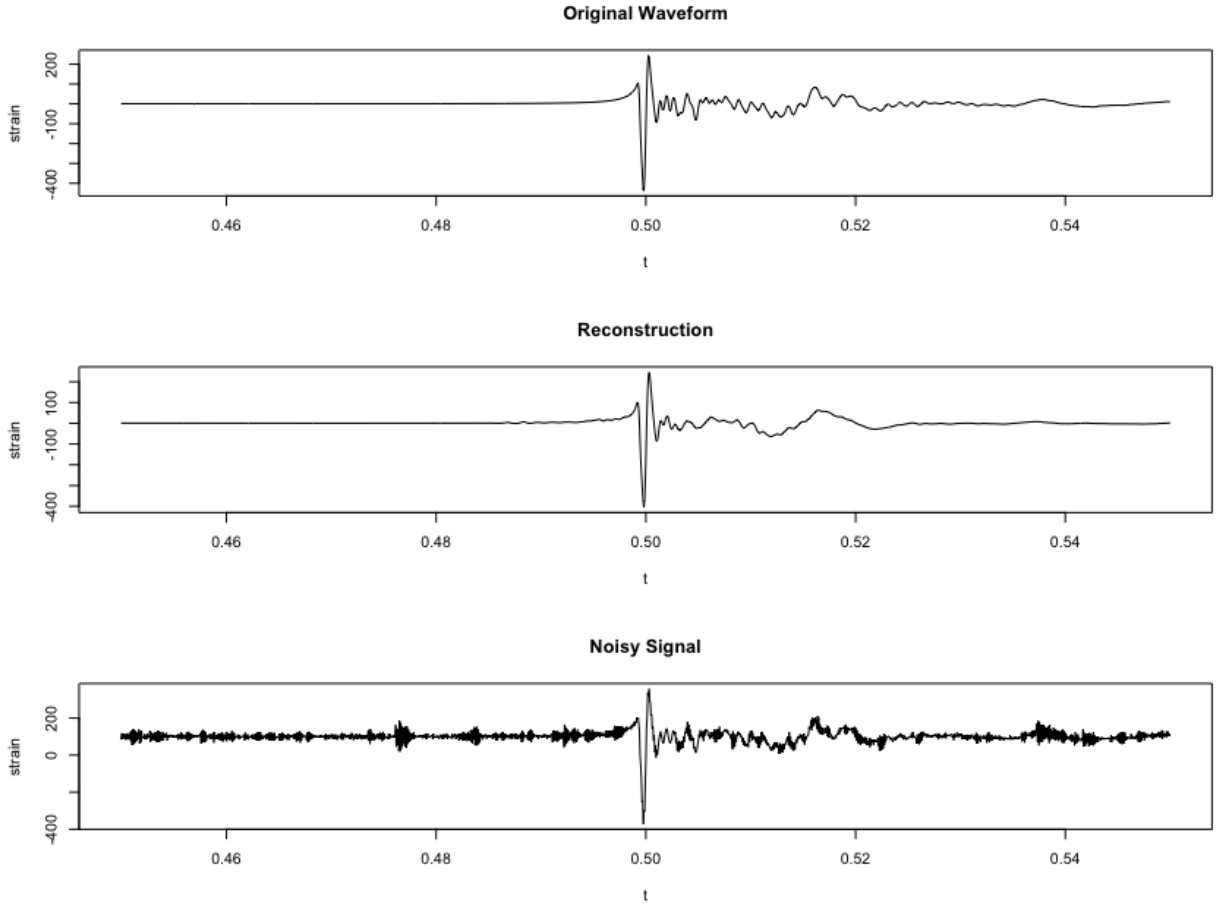

Figure 9: Noisy Signal Reconstruction with Original Waveform using 10 Principal Components

Principal component regression allows for swift reconstruction of all matched signals but presents a problem for statistical inference. The issue lies in the fact that the coefficients obtained correspond to the principal components of the waveform catalog and not the catalog itself. The principal components capture the essence of the data set, they do not correspond with any specific physical event but rather to all simulated CCSN signals used in their construction. To obtain information about the underlying physical parameters we must find a way to change the vector of PCR coefficients $\hat{\gamma}_i$ to the vector of regression coefficients $\hat{\beta}_i$

in terms of the original waveform catalog. These vectors are easily obtained using the right singular vector V obtained in the Singular Value Decomposition of the waveform catalog. Let $\hat{\gamma_i^*}$ be the vector gamma with zeros appended so that it has length 92 (the number of waveforms in the catalog). Then, $\hat{\beta}_i$, the corresponding vector of regression coefficients for the waveform catalog is given by,

$$\hat{\beta}_i = V\hat{\gamma_i^*}$$

or, in terms of matrices,

$$\hat{\beta} = V\hat{\Gamma^*}$$

where $\hat{\Gamma}^*$ is the matrix with $\hat{\gamma}_i^*$ as columns. These coefficients may now be used for hypothesis testing.

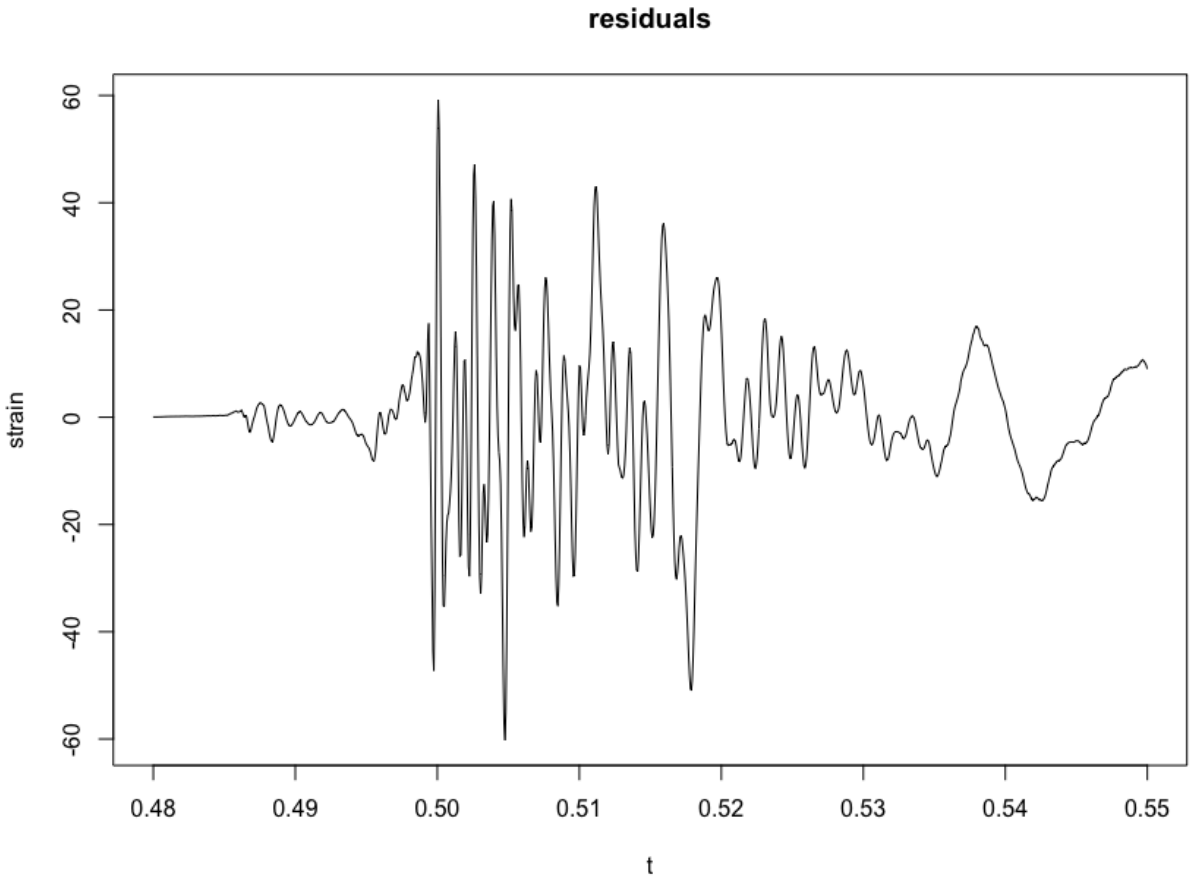

Figure 10: Residual Plot corresponding to Figure 9

3.7 Hypothesis Testing

We now seek to find which, if any, of the catalog signals best describe the reconstructed waveforms. Hypothesis tests for significance of multivariate regression coefficients are performed. The procedure for testing coefficients in a single equation from Press is applied.[Press, 2005] Under the assumption that the vector of coefficients for a single waveform are distributed as multivariate normal,

$$\mathcal{L}(\hat{\beta}_i) = N(\beta_i, \sigma_{ii}(X^T X)^{-1})$$

where X is the waveform catalog. To test if the coefficients in the ith equation for significant, or check equality to some value, Student t-tests should be used. To test $\mathbf{H} : \beta_{ij} = \beta^*_{ij}$, where β^*_{ij} is a known value, and $\beta_i = (\beta_{i1}, \beta_{i2}, \ldots, \beta_{iq})'$ and $\hat{\beta}_i = (\hat{\beta}_{i1}, \hat{\beta}_{i2}, \ldots, \hat{\beta}_{iq})'$, we use that under H,

$$\mathcal{L}\left[(\hat{\beta}_{ij} - \beta^*_{ij})/\sqrt{(w_{jj}\hat{\sigma}_{ii})}\right] = t_{N-q},$$

where

$$\hat{\sigma}_{ii} = \frac{1}{N-q}(y_i - X\hat{\beta}_i)^T(y_i - X\hat{\beta}_i)$$

and $i = 1, \ldots, p$ is the number of coefficients, $j = 1, \ldots, q$ is the number of columns and, w_{jj} is the jth diagonal element of $(X^T X)^{-1}$

Thus, for any element $\hat{\beta}_{ij}$ we obtain the t-statistic for its deviation from $\beta^*_{ij} = 0$ by evaluating,

$$t_{ij} = \hat{\beta}_{ij}/\sqrt{(w_{jj}\hat{\sigma}_{ii})}$$

Due to the high value of $N = 2^{14} \simeq N - q$, the the Student-t distribution is approximately normal. P-values are calculated by finding the are under the standard normal curve to the right of the calculated t_{ij}. This is easily performed in R using the pnorm command, although a more efficient routine could become necessary when calculating large numbers of p-values.

4 Results

Template matching between the base catalog and simulated waveforms with base and test catalog waveforms injected were performed at the $\rho_{threshold} = 0.3, 0.218,$ and 0.1 levels. The total number of template-signal combinations are $92 \times 92 = 8464$, for sets created using the base catalog, and $92 \times 47 = 4324$ for sets created using the test catalog. Cross correlations are calculated for each of the 2^{15} time steps for each of these combinations at both SNR levels. Formulating the problem in the frequency domain and using the FFT to calculate cross-correlation allows this computation to run astonishingly quickly. $2^{15} \times 92 \times 92$ cross correlations were calculated on a laptop computer in 4.7 seconds. The number of matches obtained at the different correlation thresholds for each set of simulated signals are given in Table 1. Clearly, decreasing the threshold value by small amounts in this low range has an increasingly large effect. This is visible in Figure 6 as well. Table 2 gives the number of unique injected waveforms for which matches were obtained at the different SNR levels.

		Base Catalog		Test Catalog	
Correlation Threshold	SNR	10	20	10	20
	0.3	2029	21382	1779	15208
	0.2	14645	62153	11075	38339
	0.1	88219	302661	55072	166923

Table 1: Total Number of Matches Recorded

		Base Catalog		Test Catalog	
Correlation Threshold	SNR	10	20	10	20
	0.3	45	92	27	42
	0.2	85	92	39	47
	0.1	92	92	47	47

Table 2: Number of Unique Underlying Waveforms Selected

In this analysis, false negatives should be considered much worse than false positives as we are looking for events which occur only a couple of times per century. Thus, we desire to use the lowest correlation threshold possible that maintains computational feasibility and does not trigger for simple noise glitches. In all cases presented above, the location of interest detected was close to the location at which the signal was injected (around the halfway point of the time series). It is likely that a correlation threshold between 0.2 and 0.1 is optimal but due to computational limitations signal reconstruction and hypothesis testing were only performed on the locations of interest selected out by the 0.3 correlation threshold level.

Principal Component Regression with 10 principal components was performed on the locations of interest selected by the template matching and reconstructed waveforms are generated. Using the methods described above, the coefficients from the PCR were transformed into coefficients on the base waveform catalog. Hypothesis testing for significant deviation from zero was then performed on these coefficients. P-values for these coefficients were not found to be significant at any common levels. For signals formed from waveforms from the base catalog the most significant. Thus, inferences on the importance of constituent waveforms could not be performed in the usual way. Instead of testing at levels such as $\alpha = 0.5$ or $\alpha = 0.1$, the waveform corresponding to the most significant coefficient was compared with the true underlying waveform. It was found that the correct waveform was assigned highest significance 73% for the signals with SNR 20 and 89% for signals with SNR 10. This seemingly contradictory result is likely due to the fact that only the waveforms with the most extreme features, large pre- and post- bounce deviation, were selected out by the template matching for SNR 10 at the high correlation threshold. Excluding the waveforms which were only picked out in the SNR 20 case, the correct SNR 20 match rate moves up to near 100%.

5 Conclusion and Future Work

Hypothesis testing of the coefficients recovered after PCR to find the waveforms with greatest importance and descriptive power has proven to be frustrating and disappointing and is likely a misguided approach. Fortunately, template matching as a method for detection of signals from core collapse supernovae has been shown to be both efficient and accurate. For situations where the signal is not completely swamped by the noise, template matching using the entire catalog of known waveforms efficiently detects underlying signals with a high degree of significance. This is to say, we may be confident that some signal similar to simulated CCSN signal is there but, using the methods presented in this paper, we cannot be certain about the underlying physical parameters which drove the event. Thus, template matching still may have a place in searches for CCSN as a detection method in a detection-parametrization scheme.

The issues with the statistical inference performed have many sources. One likely source of difficulty is the reliance on principal component analysis. This technique was first applied to gravitational wave astronomy by Heng (2009) as a method of speeding up signal reconstruction.[Heng, 2009] For this purpose, PCA has proven useful, but I believe it is likely unnecessary. The original catalog of waveforms is of full rank and is not particularly poorly conditioned. Its condition number is $\kappa = 130.9082$ and multiplication by its pseudo-inverse yields a matrix very close to the identity. Thus, multivariate regression with the base catalog as the data matrix could be performed. In fact, this is already essentially accomplished during template matching with each vector regressing one at a time.

In addition to applying multivariate regression, future directions would include applying some measure of similarity to the reconstructed waveform and the original underlying signal. This would allow for goodness of fit to be assessed.

References

Abbott, B. P., Abbott, R., Abbott, T., Abernathy, M., Acernese, F., Ackley, K., Adamo, M., Adams, C., Adams, T., Addesso, P., et al. (2016a). Characterization of transient noise in advanced ligo relevant to gravitational wave signal gw150914. *Classical and Quantum Gravity*, 33(13):134001.

Abbott, B. P., Abbott, R., Abbott, T., Abernathy, M., Acernese, F., Ackley, K., Adams, C., Adams, T., Addesso, P., Adhikari, R., et al. (2016b). Observation of gravitational waves from a binary black hole merger. *Physical review letters*, 116(6):061102.

Abdikamalov, E., Gossan, S., DeMaio, A. M., and Ott, C. D. (2014). Measuring the angular momentum distribution in core-collapse supernova progenitors with gravitational waves. *Physical Review D*, 90(4):044001.

Bethe, H. A. and Wilson, J. R. (1985). Revival of a stalled supernova shock by neutrino heating. *The Astrophysical Journal*, 295:14–23.

Cooley, J. W. and Tukey, J. W. (1965). An algorithm for the machine calculation of complex fourier series. *Mathematics of computation*, 19(90):297–301.

Cornish, N. J. and Littenberg, T. B. (2015). Bayeswave: Bayesian inference for gravitational wave bursts and instrument glitches. *Classical and Quantum Gravity*, 32(13):135012.

Dimmelmeier, H., Ott, C. D., Marek, A., and Janka, H.-T. (2008). Gravitational wave burst signal from core collapse of rotating stars. *Physical Review D*, 78(6):064056.

Edwards, M. (2017). *Bayesian modelling of stellar core collapse gravitational wave signals and detector noise*. PhD thesis, ResearchSpace@ Auckland.

Einstein, A. (1916). Approximative integration of the field equations of gravitation. *Sitzungsber. Preuss. Akad. Wiss. Berlin (Math. Phys.)*, 1916:688–696.

Heng, I. S. (2009). Rotating stellar core-collapse waveform decomposition: a principal component analysis approach. *Classical and Quantum Gravity*, 26(10):105005.

Lattimer, J. M. and Swesty, F. D. (1991). A generalized equation of state for hot, dense matter. *Nuclear Physics A*, 535(2):331–376.

Misner, C. W., Thorne, K. S., Wheeler, J. A., et al. (1973). Gravitation.

Ott, C., Abdikamalov, E., O'Connor, E., Reisswig, C., Haas, R., Kalmus, P., Drasco, S., Burrows, A., and Schnetter, E. (2012). Correlated gravitational wave and neutrino signals from general-relativistic rapidly rotating iron core collapse. *Physical Review D*, 86(2):024026.

Press, S. J. (2005). *Applied multivariate analysis: using Bayesian and frequentist methods of inference*. Courier Corporation.

Rencher, A. C. and Christensen, W. (2002). Méthods of multivariate analysis. a john wiley & sons. *Inc. Publication*, page 727.

Romano, J. D. and Cornish, N. J. (2017). Detection methods for stochastic gravitational-wave backgrounds: a unified treatment. *Living reviews in relativity*, 20(1):2.

Röver, C., Bizouard, M.-A., Christensen, N., Dimmelmeier, H., Heng, I. S., and Meyer, R. (2009). Bayesian reconstruction of gravitational wave burst signals from simulations of rotating stellar core collapse and bounce. *Physical Review D*, 80(10):102004.

Rowe, D. B. (2016). Image reconstruction in functional mri. *Handbook of Neuroimaging Data Analysis*, pages 205–232.

Rowe, D. B. et al. (2003). Significant fmri neurologic synchrony using monte carlo methods. *Monte Carlo Methods and Applications*, 9(4):367–386.

Shen, H., Toki, H., Oyamatsu, K., and Sumiyoshi, K. (1998). Relativistic equation of state of nuclear matter for supernova and neutron star. *Nuclear Physics A*, 637(3):435–450.

Shibata, M., Liu, Y. T., Shapiro, S. L., and Stephens, B. C. (2006). Magnetorotational collapse of massive stellar cores to neutron stars: Simulations in full general relativity. *Physical Review D*, 74(10):104026.

Woosley, S. E. and Heger, A. (2007). Nucleosynthesis and remnants in massive stars of solar metallicity. *Physics Reports*, 442(1-6):269–283.